International Journal of Computational Fluid Dynamics
Publication details, including instructions for authors and subscription information:
http://www.informaworld.com/smpp/title~content=t713455064

A parallel adaptive mesh refinement algorithm for predicting turbulent non-premixed combusting flows

X. Gao [a]; C. P. T. Groth [a]
[a] Institute for Aerospace Studies, University of Toronto, Toronto, Ont., Canada

Online Publication Date: 01 June 2006

To cite this Article: Gao, X. and Groth, C. P. T. (2006) 'A parallel adaptive mesh refinement algorithm for predicting turbulent non-premixed combusting flows', International Journal of Computational Fluid Dynamics, 20:5, 349 — 357

To link to this article: DOI: 10.1080/10618560600917583
URL: http://dx.doi.org/10.1080/10618560600917583

International Journal of Computational Fluid Dynamics, Vol. 20, No. 5, June 2006, 349–357

Taylor & Francis
Taylor & Francis Group

A parallel adaptive mesh refinement algorithm for predicting turbulent non-premixed combusting flows

X. GAO* and C.P.T. GROTH†

Institute for Aerospace Studies, University of Toronto, 4925 Dufferin Street, Toronto, Ont., Canada M3H 5T6

(Received 2 August 2005; in final form 20 July 2006)

A parallel adaptive mesh refinement (AMR) algorithm is proposed for predicting turbulent non-premixed combusting flows characteristic of gas turbine engine combustors. The Favre-averaged Navier–Stokes equations governing mixture and species transport for a reactive mixture of thermally perfect gases in two dimensions, the two transport equations of the $k-\omega$ turbulence model, and the time-averaged species transport equations, are all solved using a fully coupled finite-volume formulation. A flexible block-based hierarchical data structure is used to maintain the connectivity of the solution blocks in the multi-block mesh and facilitate automatic solution-directed mesh adaptation according to physics-based refinement criteria. This AMR approach allows for anisotropic mesh refinement and the block-based data structure readily permits efficient and scalable implementations of the algorithm on multi-processor architectures. Numerical results for turbulent non-premixed diffusion flames for a bluff-body burner are described and compared to available experimental data. The numerical results demonstrate the validity and potential of the parallel AMR approach for predicting complex non-premixed turbulent combusting flows.

Keywords: Parallel computing; Adaptive mesh refinement; Turbulent combustion; Non-premixed flames

Nomenclature

$A_{i,j}$	area of cell i, j
$\vec{u}$	Favre-averaged mixture velocity
c_{p_n}	species specific heat
c_n	species mass fraction
D_b	bluff-body burner diameter
D_k	diffusion coefficient for turbulent energy
D_{t_n}	turbulent diffusivity of species n
e	Favre-averaged total specific mixture energy
E_p	relative parallel efficiency
$\vec{f}$	body force per unit volume
$\mathbf{F}$	inviscid radial flux vector
$\mathbf{F}_\mathrm{v}$	viscous radial flux vector
$\mathbf{G}$	inviscid axial flux vector
$\mathbf{G}_\mathrm{v}$	viscous axial flux vector
h_n	absolute internal enthalpy for species n
$\vec{\mathcal{J}}_n$	species molecular diffusive flux
$\vec{\mathcal{J}}_{\mathrm{t}_n}$	species turbulent diffusive flux
k	specific turbulent kinetic energy
Ma	Mach number
N	total number of species
p	time-averaged mixture pressure
Pr_t	turbulent Prandtl number
$\vec{n}$	unit vector normal to the cell face or edge
$\vec{q}$	molecular heat flux vector
$\vec{q}_\mathrm{t}$	turbulent heat flux vector
r	radial coordinate of the axisymmertric frame
Re	Reynolds number
$\mathbf{S}$	source vector
Sc_t	turbulent Schmidt number
S_{ki}	strain rate tensor
S_p	relative parallel speed-up
$\mathbf{S}_\phi$	inviscid source vector
$\mathbf{S}_{\phi_\mathrm{v}}$	viscous source vector
u_τ	friction velocity
v_r	radial Favre-averaged velocity component
v_z	axial Favre-averaged velocity component
y	the distance normal from the wall
y^+	dimensionless, normal distance from wall

*Corresponding author. Email: gao@utiasutoronto.ca
† Email: groth@utias.utoronto.ca

International Journal of Computational Fluid Dynamics
ISSN 1061-8562 print/ISSN 1029-0257 online © 2006 Taylor & Francis
http://www.tandf.co.uk/journals
DOI: 10.1080/10618560600917583

z	axial coordinate of the axisymmertric frame
$\Delta\ell$	length of the cell face

Greek Symbols

α, β, $\beta*$, σ, $\sigma*$	closure coefficients of $k-\omega$ two-equation model
$\vec{\vec{\lambda}}$	turbulent Reynolds stress tensor or dyad
μ	mixture molecular viscosity
μ_n	species molecular viscosity
μ_t	eddy viscosity
ρ	time-averaged mixture density
τ_w	wall shear stress
κ	thermal conductivity
κ_n	species thermal conductivity
κ_t	turbulent thermal conductivity
$\vec{\vec{\tau}}$	molecular stress tensor or dyad
ω	specific dissipation rate
Ω_{ij}	vorticity tensor
$\dot{w}_n$	species mean reaction rate

1. Introduction

In the last twenty years, numerical methods have become an essential tool for the investigation of turbulent combusting flows. Due to more manageable computational requirements and somewhat greater ease in handling complex flow geometries, most practical simulation algorithms are based on the Reynolds- or Favre-averaged Navier–Stokes equations, where the turbulent flow structure is entirely modelled and not resolved. In spite of simplifications offered by the time-averaging approach, the system of equations governing turbulent combusting flows can be both large and stiff and its solution can still place severe demands on available computational resources.

Many approaches have been taken to reduce the computational costs of simulating combusting flows. One successful approach is to make use of solution-directed mesh adaptation, such as the adaptive mesh refinement (AMR) algorithms developed for aerospace applications (Berger 1984, Berger and Colella 1989, Quirk 1991, De Zeeuw and Powell 1993, Powell *et al.* 1993, Quirk and Hanebutte 1993, Berger and Saltzman 1994, Aftosmis *et al.* 1998, Groth *et al.* 1999, 2000, Sachdev *et al.* 2005). Computational grids that automatically adapt to the solution of the governing equations are very effective in treating problems with disparate length scales, providing the required spatial resolution while minimising memory and storage requirements. Recent progress in the development and application of AMR algorithms for low-Mach-number reacting flows and premixed turbulent combustion is described by Bell *et al.* (2001, 2002) and Bell (2004). Another approach for coping with the computational cost of reacting flow prediction is to apply a domain decomposition procedure and solve the problem in a parallel fashion using multiple processors. Large massively parallel distributed-memory computers can provide many fold increases in processing power and memory resources beyond those of conventional single-processor computers and would, therefore, provide an obvious avenue for greatly reducing the time required to obtain numerical solutions of combusting flows. Douglas *et al.* (1998) describe a parallel algorithm for numerical combustion modelling. More recently, Northrup and Groth (2005) combined these two numerical approaches, producing a parallel AMR method that both reduces the overall problem size and the time to calculate a solution for laminar combusting flows. The extension of this combined approach to turbulent non-premixed combusting flows is the focus of this study.

2. Mathematical model of turbulent combusting flows

2.1 Favre-averaged Navier–Stokes equations

A mathematical model based on the Favre-averaged Navier–Stokes equations for a compressible thermally perfect reactive mixture of gases has been formulated and is used herein to describe turbulent non-premixed combustion processes. In this formulation, the continuity, momentum and energy equations for the reactive mixture of N species are

$$\frac{\partial \rho}{\partial t} + \vec{\nabla}\cdot(\rho\vec{u}) = 0, \tag{1}$$

$$\frac{\partial}{\partial t}(\rho\vec{u}) + \vec{\nabla}\cdot\left(\rho\vec{u}\vec{u} + p\vec{\vec{I}}\right) = \vec{\nabla}\cdot\left(\vec{\vec{\tau}} + \vec{\vec{\lambda}}\right) + \vec{f}, \tag{2}$$

$$\begin{aligned}\frac{\partial}{\partial t}(\rho e) + \vec{\nabla}\cdot\left[\rho\vec{u}\left(e + \frac{p}{\rho}\right)\right] =& \vec{\nabla}\cdot\left[\left(\vec{\vec{\tau}} + \vec{\vec{\lambda}}\right)\cdot\vec{u}\right] \\ &+ \vec{\nabla}\cdot(D_k\vec{\nabla}_k) \\ &- \vec{\nabla}\cdot(\vec{q} + \vec{q}_t) + \vec{u}\cdot\vec{f},\end{aligned} \tag{3}$$

where ρ is the time-averaged mixture density, $\vec{u}$ is the Favre-averaged mean velocity of the mixture, p is the time-averaged mixture pressure, $e = |\vec{u}|^2/2 + \sum_{n=1}^{N} c_n h_n - p/\rho + k$ is the Favre-averaged total specific mixture energy, $\vec{f}$ is a body force per unit volume acting on the gaseous mixture, k is the specific turbulent kinetic energy, D_k is the coefficient for the diffusion of the turbulent energy, $\vec{\vec{\tau}}$ and $\vec{\vec{\lambda}}$ are the molecular and turbulent Reynolds stress tensors or dyads, and $\vec{q}$ and $\vec{q}_t$ are the molecular and turbulent heat flux vectors, respectively. Fourier's law is used to represent the thermal diffusion caused by the random thermal motion and turbulence. In addition, h_n is the absolute (chemical and sensible) internal enthalpy for species n. The transport equation

describing the time evolution of the species mass fraction, c_n, is given by

$$\frac{\partial}{\partial t}(\rho c_n) + \vec{\nabla}\cdot(\rho c_n \vec{u}) = -\vec{\nabla}\cdot(\vec{\mathcal{J}}_n + \vec{\mathcal{J}}_{t_n}) + \rho \dot{w}_n, \quad (4)$$

where $\dot{w}_n$ is the time-averaged or mean rate of the change of the species mass fraction produced by the chemical reactions and $\vec{\mathcal{J}}_n$ and $\vec{\mathcal{J}}_{t_n}$ are the molecular and turbulent diffusive fluxes for species n, respectively. The latter are specified using Fick's law. The modified two-equation $k-\omega$ model of Wilcox (2002) is used here to model the unresolved turbulent flow quantities. In this approach, the Boussinesq approximation is used to relate the Reynolds stress tensor, $\vec{\vec{\lambda}}$, to the mean flow strain-rate tensor using a turbulent eddy viscosity, μ_t, with $\mu_t = \rho k/\omega$. Transport equations are solved for turbulent kinetic energy, k, and the specific dissipation rate, ω, given by

$$\frac{\partial}{\partial t}(\rho k) + \vec{\nabla}\cdot(\rho k \vec{u}) = \vec{\vec{\lambda}}\colon \vec{\nabla}\vec{u} + \vec{\nabla}\cdot[(\mu + \mu_t \sigma^*)\vec{\nabla} k] - \beta^* \rho k \omega, \quad (5)$$

$$\frac{\partial}{\partial t}(\rho \omega) + \vec{\nabla}\cdot(\rho \omega \vec{u}) = \alpha \frac{\omega}{k}\vec{\vec{\lambda}}\colon \vec{\nabla}\vec{u} + \vec{\nabla}\cdot[(\mu + \mu_t \sigma)\vec{\nabla}\omega] - \beta \rho \omega^2, \quad (6)$$

where μ is the molecular viscosity of the mixture and $\beta*$, $\sigma*$, α, β and σ are closure coefficients of this two-equation model. The latter are given by

$$\alpha = \frac{13}{25}, \quad \beta = \beta_0 f_\beta, \quad \beta^* = \beta_0^* f_{\beta^*}, \quad \sigma = \sigma^* = \frac{1}{2}, \quad (7)$$

with

$$\beta_0 = \frac{9}{125}, \quad \beta_0^* = \frac{9}{100}, \quad (8)$$

$$f_\beta = \frac{1 + 70\chi_\omega}{1 + 80\chi_\omega}, \quad f_{\beta^*} = \begin{cases} 1 & \chi_k \le 0, \\ \frac{1+680\chi_k^2}{1+400\chi_k^2} & \chi_k > 0, \end{cases} \quad (9)$$

and $\chi_\omega = |\Omega_{ij}\Omega_{jk}S_{ki}/(\beta_0^*\omega)^3|$, $\chi_k = (\partial k/\partial x_j)(\partial \omega/\partial x_j)/\omega^3$. The tensors Ω_{ij} and S_{ki} are the vorticity and strain rate tensors, respectively.

For two-dimensional axisymmetric flows, the preceding equations can be re-expressed using vector notation as

$$\frac{\partial \mathbf{U}}{\partial t} + \frac{\partial}{\partial r}(\mathbf{F} - \mathbf{F}_v) + \frac{\partial}{\partial z}(\mathbf{G} - \mathbf{G}_v) = \frac{1}{r}(\mathbf{S}_\phi + \mathbf{S}_{\phi_v}) + \mathbf{S} \quad (10)$$

where $\mathbf{U}$ is the vector of conserved variables given by

$$\mathbf{U} = [\rho, \rho v_r, \rho v_z, \rho e, \rho k, \rho \omega, \rho c_1, \ldots, \rho c_N]^T, \quad (11)$$

and $\mathbf{F}$ and $\mathbf{F}_v$ are the inviscid and viscous radial flux vectors, $\mathbf{G}$ and $\mathbf{G}_v$ are the inviscid and viscous axial flux vectors, $\mathbf{S}_\phi$ and $\mathbf{S}_{\phi_v}$ are the inviscid and viscous source vectors associated with the axisymmetric geometry, and $\mathbf{S}$ is the source vector containing terms related to the finite rate chemistry, body forces, and turbulence modelling, respectively. Here, r and z are the radial and axial coordinates of the axisymmertric frame and v_r and v_z are the radial and axial velocity components.

2.2 Thermodynamic and transport properties

Thermodynamic relationships and transport coefficients are required to close the system of equations given above. Thermodynamic and molecular transport properties of each gaseous species are prescribed using the empirical database compiled by Gordon and McBride (1994) and McBride and Gordon (1996), which provides curve fits for the species enthalpy, h_n, specific heat, c_{p_n}, entropy, viscosity, μ_n, and thermal conductivity, κ_n, as functions of temperature. The molecular viscosity, μ, and thermal conductivity, κ, of the reactive mixture are determined using the mixture rules of Wilke (1950) and Mason and Saxena (Dixon-Lewis 1984), respectively. Turbulent contributions to thermal conductivity and species diffusivity are modelled by making an analogy between momentum and heat transfer and introducing the turbulent Prandtl and Schmidt numbers, Pr_t and Sc_t, both of which are taken to be constant ($Pr_t = 0.9$ and $Sc_t = 1$), and assuming $\kappa_t = \mu_t c_p/Pr_t$ and $D_{t_n} = \mu_t/\rho Sc_t$.

2.3 Reduced chemical kinetics and eddy dissipation model

For methane-air combustion considered in the presented work, the following reduced, one-step, five-species, chemical kinetic scheme of Westbrook and Dryer (1981) is used:

$$CH_4 + 2O_2 \rightarrow CO_2 + 2H_2O. \quad (12)$$

The five species are methane (CH_4), oxygen (O_2), carbon dioxide (CO_2), water (H_2O) and nitrogen (N_2). Nitrogen is taken to be inert.

In order to account for the strong interaction that exists between the chemistry and turbulence in non-premixed combustion processes, the mean reaction rate, $\dot{w}_n$, is estimated using the eddy dissipation model (EDM) of Magnussen and Hjertager (1976). This model assumes that turbulence mixing limits the fuel burning and the fuel reaction rate is limited by the deficient species. The individual species mean reaction rate is then taken to be the minimum of the rates given by the finite-rate chemical kinetics (i.e. the law of mass action and Arrhenius reaction rates) and the EDM value. The latter is related to the turbulence mixing time and is estimated using the dissipation rate, ω.

2.4 Treatment of near-wall turbulence

Both low-Reynolds-number and wall-function formulations of the $k-\omega$ model are used for the treatment of

near-wall turbulent flows, with a procedure for automatically switching from one to the other, depending on mesh resolution. In the case of the low-Reynolds-number formulation, it can be shown that

$$\lim_{y\to 0}\omega = \frac{6\nu}{\beta y^2} \tag{13}$$

where y is the distance normal from the wall. Rather than attempting to solve the ω-equation directly, the preceding expression is used to specify ω for all values of $y^+ \leq 2.5$, where $y^+ = u_\tau y/\nu$, $u_\tau^2 = \tau_w/\rho$, and τ_w is the wall shear stress. Provided there are 3–5 computational cells inside $y^+ = 2.5$, this procedure reduces numerical stiffness, guarantees numerical accuracy, and permits the k–ω model to be solved directly in the near-wall region without resorting to wall functions. In the case of the wall-function formulation, the expressions

$$k = \frac{u_\tau^2}{\sqrt{\beta_0^*}} \tag{14}$$

$$\omega = \frac{u_\tau}{\sqrt{\beta_0^*}\kappa y} \tag{15}$$

are used to fully specify k and ω for $y^+ \leq 30$–250, where κ is the von Kármán constant. The formulae

$$k = \frac{u_\tau^2}{\sqrt{\beta_0^*}}\left(\frac{y^+}{y^+_{\text{cutoff}}}\right)^2 \tag{16}$$

$$\omega = \omega_0\sqrt{1+\left(\frac{\omega_{\text{wall}}}{\omega_0^2}\right)^2} \tag{17}$$

have been devised to prescribe k and ω for y^+ lying between 2.5 and a cutoff value, y^+_{cutoff}, where ω_0 and ω_{wall} are the values in the near-wall sublayer and in the log layer, respectively. The cutoff, y^+_{cutoff}, is taken to be in the range 30–50 for this study. When y^+ is close to the lower limit, 2.5, k and ω approach zero and the asymptotic value, respectively. When y^+ approaches y^+_{cutoff}, the wall function is recovered. This automatic near-wall treatment readily accommodates situations during AMR where the mesh resolution may not be sufficient for directly calculating near-wall turbulence using the low-Reynolds-number formulation.

3. Parallel AMR algorithm

3.1 Finite volume scheme

A finite volume scheme is employed to solve the Favre-averaged Navier–Stokes equations of equation (10) above for a two-dimensional axisymmetric coordinate frame. The system of governing equations is integrated over quadrilateral cells of a structured multi-block quadrilateral mesh. The semi-discrete form of this finite-volume formulation applied to cell (i, j) is given by

$$\frac{d\mathbf{U}_{i,j}}{dt} = -\frac{1}{A_{i,j}}\sum_{\text{faces},k}\vec{\mathbf{F}}_{i,j,k}\cdot\vec{n}_{i,j,k}\Delta\ell_{i,j,k} + \frac{1}{r_{i,j}}\left(\mathbf{S}_{\phi_{i,j}} + \mathbf{S}_{\phi_{v_{i,j}}}\right) + \mathbf{S}_{i,j}, \tag{18}$$

where $\vec{\mathbf{F}} = (\mathbf{F} - \mathbf{F}_v, \mathbf{G} - \mathbf{G}_v)$, $r_{i,j}$ and $A_{i,j}$ are the radius and area of cell (i, j), and $\Delta\ell$ and $\vec{n}$ are the length of the cell face and unit vector normal to the cell face or edge, respectively. The inviscid (hyperbolic) components of the numerical flux at each cell face is evaluated using limited linear reconstruction (Barth 1993) and one of several Riemann-solver based flux functions (Roe 1981, Einfeldt 1988, Linde 2002). The viscous (elliptic) components of the cell face flux are evaluated by employing a centrally-weighted diamond-path reconstruction procedure as described by Coirier and Powell (1996).

For the time-invariant calculations performed as part of this study, a multigrid algorithm with multi-stage time marching scheme smoother is used to solve the coupled set of non-linear ordinary differential equations that arise from the finite-volume spatial discretization procedure. The smoother is based on the optimally-smoothing multi-stage time marching schemes developed by van Leer *et al.* (1989). To cope with numerical stiffness, a semi-implicit treatment is used in the temporal discretization of the source terms associated with axisymmetric geometry, finite-rate chemistry, turbulence modelling, and gravitational acceleration.

3.2 Block-based adaptive mesh refinement

AMR algorithms, which automatically adapt the mesh to the solution of the governing equations, can be very effective in treating problems with disparate length scales. They permit local mesh refinement and thereby minimise the number of computational cells required for a particular calculation. Following the approach developed by Groth *et al.* (1999, 2000) for computational magnetohydrodynamics, a flexible block-based hierarchical data structure has been developed and is used in conjunction with the finite-volume scheme described above to facilitate automatic solution-directed mesh adaptation on multi-block body-fitted quadrilateral mesh according to physics-based refinement criteria. The method allows for anisotropic mesh refinement and is well suited to parallel implementation via domain decomposition. Refer to the recent papers by Sachdev *et al.* (2005) and Northrup and Groth (2005) for further details.

3.3 Domain decomposition and parallel implementation

A parallel implementation of the block-based AMR scheme has been developed using the C++ programming language and the message passing interface (MPI) library

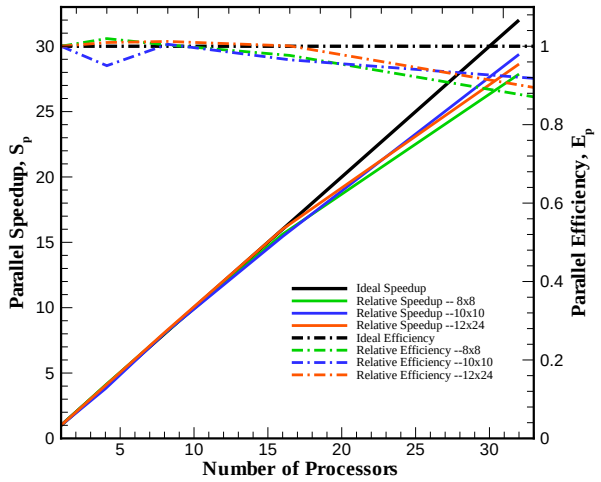

Figure 1. Relative parallel speed-up, S_p, and efficiency, E_p, for a fixed-size problem using up to 32 processors.

by Gropp *et al.* (1999). A domain decomposition procedure is used where the solution blocks making up the computational mesh are distributed equally among available processors, with more than one block permitted per processor. A Morton ordering space filling curve is used to order the blocks for more efficient load balancing (Aftosmis *et al.* 2004).

The parallel implementation has been carried out on a parallel cluster of 4-way Hewlett-Packard ES40, ES45, and Integrity rx4640 servers with a total of 244 Alpha and Itanium 2 processors. A low-latency Myrinet network and switch is used to interconnect the servers in the cluster. Estimates of the parallel performance and scalability of the proposed solution-adaptive method on this facility are shown in figure 1 for a fixed-size turbulent non-reacting multi-species flow problem having 64 solution blocks. The relative parallel speed-up, S_p, defined as

$$S_p = \frac{t_1}{t_p} p, \tag{19}$$

and the relative parallel efficiency, E_p, defined as

$$E_p = \frac{S_p}{p}, \tag{20}$$

are both shown in the figure, where t_1 is the processor time required to solve the problem using a single processor, and t_p is the total processor time required to solve the problem using p processors. The performance indicators are shown for three different mesh sizes: 4096 cells (64 8 × 8 cell blocks); 6400 cells (64 10 × 10 cell blocks); and 18,432 cells (64 12 × 24 cell blocks). It can be seen that the parallel speed-up of block-based AMR scheme is nearly linear and is about 87% for up to 32 processors, even for the smaller 8 × 8 cell solution blocks. The parallel efficiency is 92% for the larger 10 × 10 cell solution blocks.

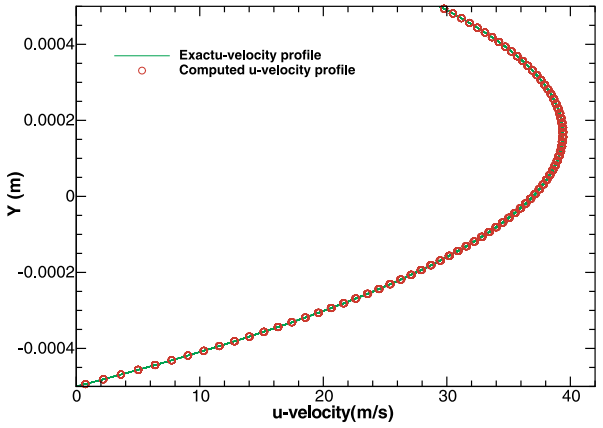

Figure 2. Comparison of predicted and exact solutions of the axial velocity profile for laminar Couette flow.

4. Numerical verification and validation

4.1 Non-reacting laminar Couette flow

The validation and verification of the proposed parallel AMR scheme has been carried out for laminar flows (Northrup and Groth 2005). The computation of non-reacting laminar Couette flow in a channel with a moving wall was considered in order to demonstrate the accuracy of the viscous spatial discretization scheme. The case with an upper wall velocity of $29.4\,\mathrm{m\,s^{-1}}$ and a favourable pressure gradient of $\mathrm{d}p/\mathrm{d}x = -3177\,\mathrm{Pa\,m^{-1}}$ was investigated and compared to the analytic solution. The predicted velocity profile is plotted and compared to the exact analytic solution for this incompressible isothermal flow in figure 2 for a uniform mesh consisting of 3200 cells with 80 cells across the channel. The L_1- and L_2-norms of the error in axial component of velocity are plotted in figure 3. The slopes of the two norms are 2.02 and 1.95, respectively, indicating that the finite-volume scheme is indeed second-order accurate. The proposed scheme has also been found to provide predictions of axisymmetric

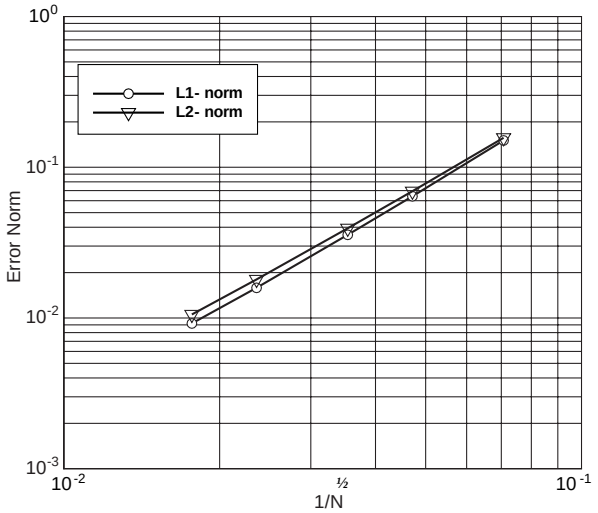

Figure 3. L_1- and L_2-norms of the solution error for laminar Couette flow.

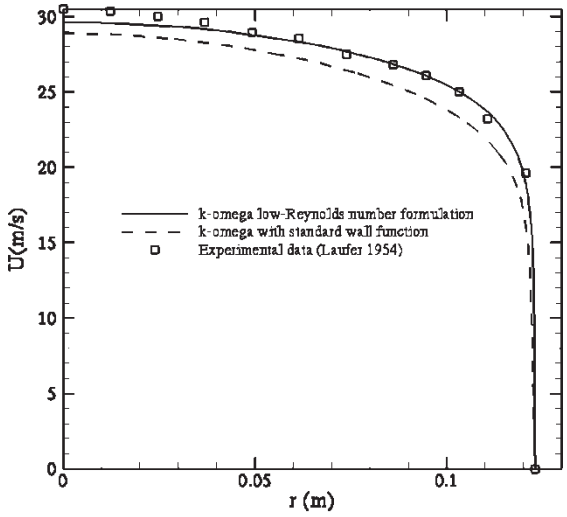

Figure 4. Comparison of predicted mean axial velocity with experimental data for fully developed turbulent pipe flow, $Re = 500{,}000$.

co-flow methane-air diffusion flames that are in good agreement with experimental data.

4.2 Fully-developed turbulent pipe flow

The validation of the parallel AMR scheme for non-reacting turbulent flows has also been considered by comparing numerical results to the experimental data of Laufer (1954) for non-reacting, fully-developed turbulent flow in a pipe with $Re = 500{,}000$. Solutions for both the wall function and low-Reynolds-number formulations of the $k-\omega$ turbulence model are compared to measured mean axial velocity and turbulent kinetic energy profiles in figures 4 and 5. Calculations with the low-Reynolds-number formulation were performed using 80 cells in the radial direction with 3–4 of those cells lying within the laminar sublayer. The first cell off the wall was located at $y^+ \approx 0.6$. The results using the wall functions was obtained using 32 cells in the radial

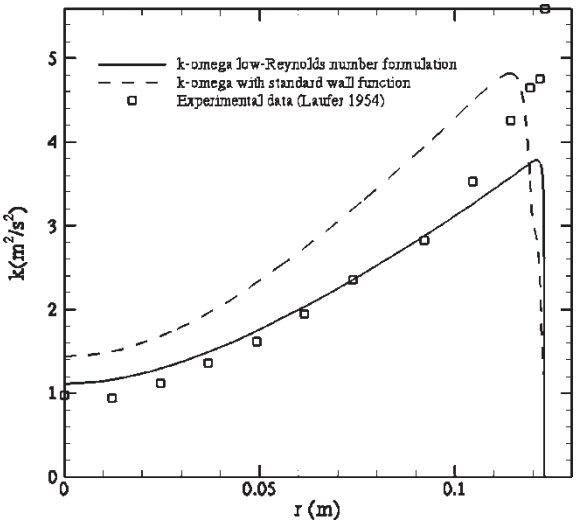

Figure 5. Comparison of predicted turbulent kinetic energy with experimental data for fully developed turbulent pipe flow, $Re = 500{,}000$.

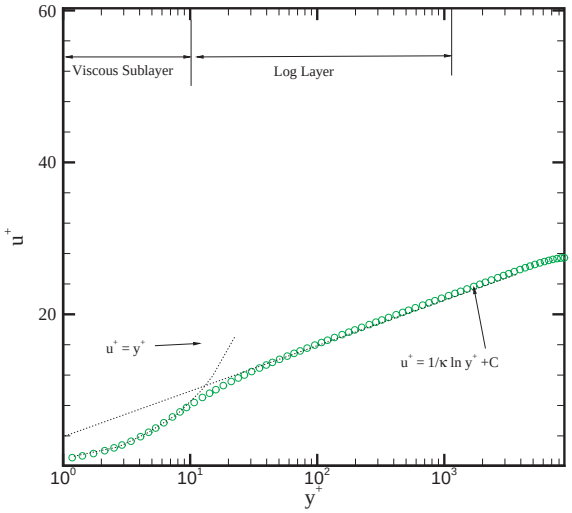

Figure 6. Predicted mean axial velocity profile in the near-wall region of fully developed pipe flow, $Re = 500{,}000$.

direction with the first cell located at $y^+ \approx 43$. The agreement between the experimental data and numerical results for this case is generally quite good. As expected, it is evident that the $k-\omega$ model is able to reproduce the characteristic features of fully-developed pipe flow and, in particular, figure 6 shows that the predictions using the low-Reynolds-number model are in excellent agreement with well-established theoretical results in the near-wall region.

5. Numerical results for bluff-body burner

5.1 Non-reacting flow

The International Workshops on Measurement and Computation of Turbulent Non-Premixed Flames (TNF) have lead to the establishment of an Internet library of

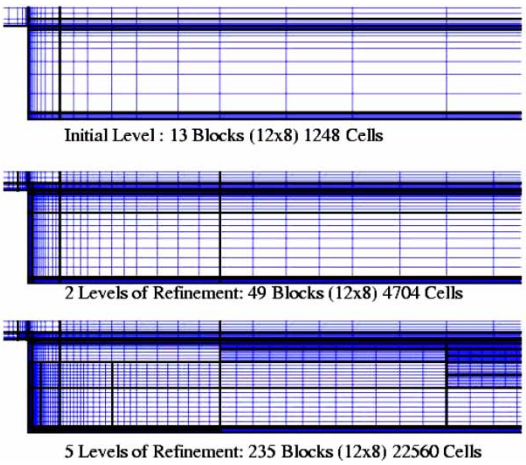

Figure 7. The initial mesh consisted of 13 12 × 8 cell blocks and 1248 cells and the final mesh consisted of 235 12 × 8 cell blocks and 22,560 cells after five levels of refinement.

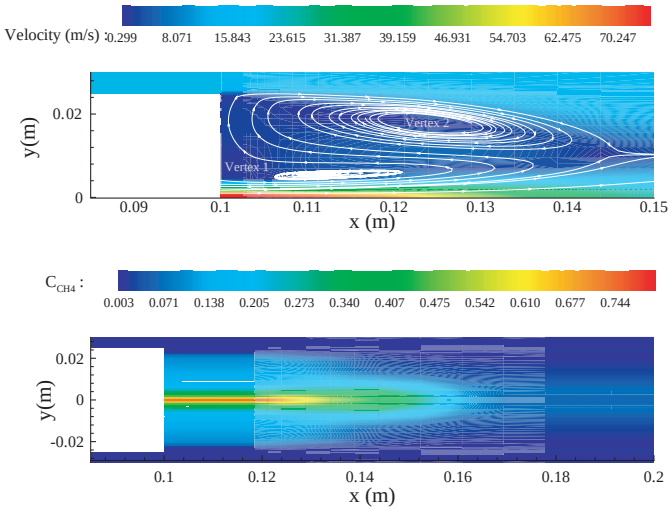

Figure 8. Predicted flow velocity, streamlines, and CH_4 mass fraction for non-reacting flow fields of the bluff-body burner.

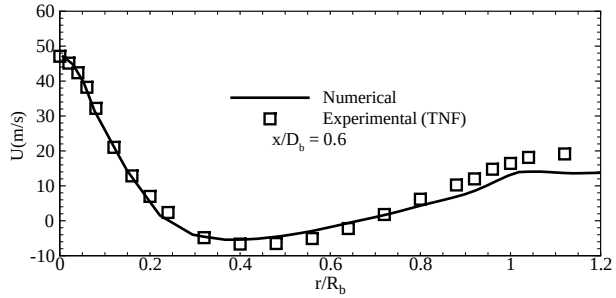

Figure 9. Comparison of predicted and measured axial velocity component at $x/D_b = 0.6$ downstream from the base of the bluff-body for non-reacting bluff-body burner with air jet.

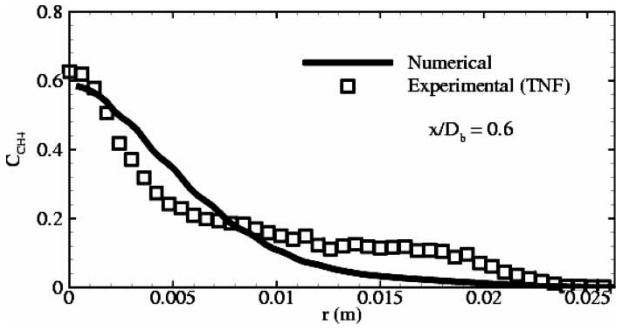

Figure 10. Comparison of predicted and measured mass fractions of CH_4 at $x/D_b = 0.6$ downstream from the base of the bluff-body for non-reacting bluff-body burner with methane jet.

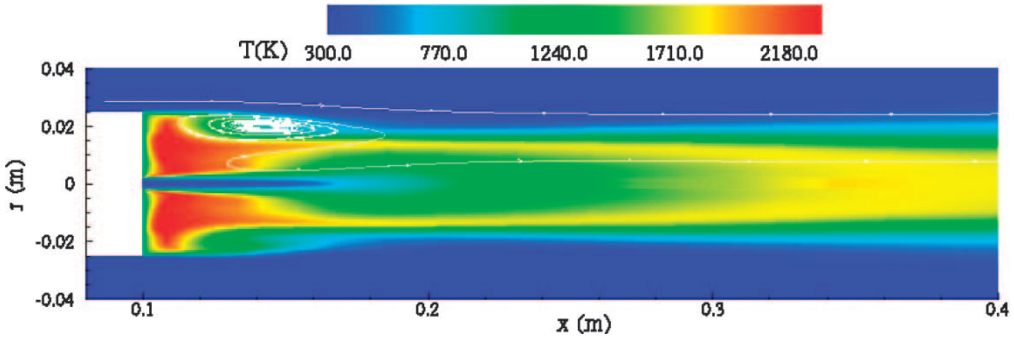

Figure 11. Predicted mean temperature distribution for combusting flow field of the bluff-body burner.

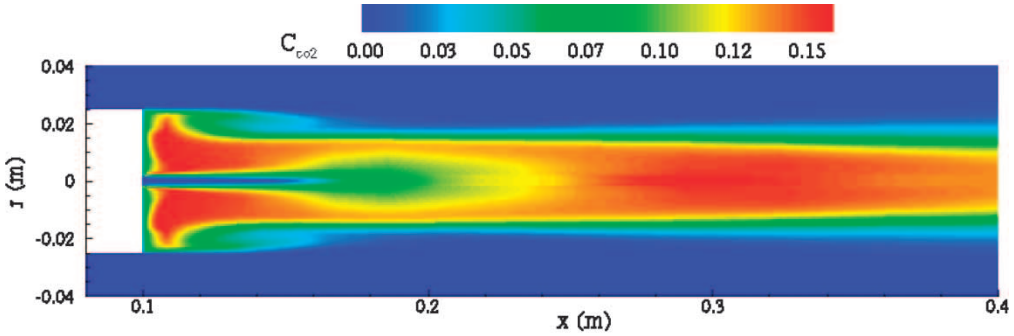

Figure 12. Predicted distribution of the mass fraction of CO_2 for combusting flow field of the bluff-body burner.

well-documented TNF that are appropriate for combustion model validation. Following the initial validation efforts described above, the proposed parallel AMR method was applied to the solution of two non-reacting flow cases associated with the bluff-body burner configuration that forms part of this experimental database. These bluff-body jet flows have been investigated and/or used for validation purposes in several recent studies by Dally *et al.* (1998) and Turpin and Troyes (2000). For the cases considered, the diameter of the bluff-body is $D_b = 50\,\text{mm}$ and the velocity and temperature of the co-flowing air is $20\,\text{m s}^{-1}$ and 300 K, respectively. In the first case of interest, air is injected through an orifice of diameter 3.6 mm at the base of the cylindrical bluff-body with a temperature of 300 K and velocity of $61\,\text{m s}^{-1}$. The Reynolds and Mach numbers based on the high-speed jet are $Re = 193{,}000$ and $Ma = 0.18$. In the second case, methane is injected at the base of the bluff-body with a velocity of $50\,\text{m s}^{-1}$ and a temperature of 300 K. In this case, the Reynolds and Mach numbers based on the methane flow are $Re = 145{,}000$ and $Ma = 0.11$.

Figure 8 shows the predicted mean velocity, streamlines, and methane mass fraction for both the air and methane fuel jets obtained using a mesh consisting of 235 12 × 8 cell blocks and 22,560 cells with five levels of refinement. The sequence of adaptively refined grids for these two cases is shown in figure 7. For the air jet case, the flow field predictions are generally in good agreement with the experimental data (not shown) and reveal the formation of a double-vortex structure in the re-circulation zone which are important in controlling fuel/oxidiser mixing. A comparison of the predicted radial profile of the axial velocity component at $x/D_b = 0.6$ downstream from the base of the bluff-body to the measured data is given in figure 9. Again, good agreement between the numerical predictions and experiment can be observed. For the methane jet case, the predictions of the mixing field is also found to be quite reasonable. Figure 10 shows a comparison of the predicted and measured radial profile of the mass fractions of CH_4 at $x/D_b = 0.6$ downstream from the base of the bluff-body.

5.2 Reacting flow

The numerical solution of a methane-air combusting flow field for the bluff-body burner described above has also been considered here. The flow geometry and boundary conditions for this reacting case are the same as those for the non-reacting cases, except that the velocities of the co-flowing air and methane fuel are 25 and $108\,\text{m s}^{-1}$, respectively. The Reynolds and Mach numbers are $Re = 315{,}000$ and $Ma = 0.24$. Computations were carried out using a mesh consisting of 97 16 × 16 cell blocks and 24,832 cells with four levels of refinement.

Figures 11 and 12 show the predicted distributions of mean temperature and mean mass fraction of CO_2 for this turbulent non-premixed flame. The predicted flame structure is generally in agreement with the experimentally observed structure. The flame is quite elongated and three zones can be identified: the re-circulation, neck and jet-like propagation zones. The predicted mean temperature, 1350 K and mass fraction of CO_2, 0.1, at location of ($x/D_b = 1.92$, $r/R_b = 0.4$) are compared to the measured values of the flame temperature, 1120 K, and carbon dioxide concentration, 0.07. The temperature and hence carbon dioxide concentration are somewhat over-predicted. However, the agreement with the experimental values is reasonable considering the limitations of the simplified reduced chemical kinetics scheme and turbulence/chemistry interaction model used herein, as well as the fact that radiation transport is not taken into account in the simulation.

6. Concluding remarks

A highly parallelized AMR scheme has been described for turbulent non-premixed combusting flows. The combination of a block-based AMR strategy and parallel implementation has resulted in a powerful computational tool, as demonstrated by the non-reacting and reacting flow results for the turbulent non-premixed flame bluff body burner. Future work will involve the extension of the algorithm to three-dimensional flow geometries and the application to more realistic combustor configurations.

Acknowledgements

This research was supported by a Collaborative Research Opportunities Grant from the Natural Sciences and Engineering Research Council of Canada. Funding for the parallel computing facility used to perform the computations described herein was obtained from the Canadian Foundation for Innovation and Ontario Innovation Trust (CFI Project No. 2169). The authors are very grateful to these funding agencies for this support.

References

Aftosmis, M.J., Berger, M.J. and Melton, J.E., Robust and efficient Cartesian mesh generation for component-base geometry. *AIAA J.*, 1998, **36**, 952–960.

Aftosmis, M.J., Berger, M.J. and Murman, S.M., Applications of space-filling curves to Cartesian methods for CFD. *AIAA Pap.*, 2004, 2004–1232.

Barth, T.J., Recent developments in high order k-exact reconstruction on unstructured meshes. *AIAA Pap.*, 1993, 93–668.

Bell, J.B., AMR for low Mach number reacting flow, 2004, http://repositories.cdlib.org/lbnl/LBNL-54351.

Bell, J.B., Day, M.S., Almgren, A.S., Lijewski, M.J. and Rendleman, C.A., Adaptive numerical simulation of turbulent premixed combustion. In *Proceedings of the First MIT Conference on Computational Fluid and Solid Mechanics*, June 2001.

Bell, J.B., Day, M.S., Almgren, A.S., Lijewski, M.J. and Rendleman, C.A., A parallel adaptive projection method for low Mach number flows. *Int. J. Numer. Meth. Fluids*, 2002, **40**, 209–216.

Berger, M.J., Adaptive mesh refinement for hyperbolic partial differential equations. *J. Comput. Phys.*, 1984, **53**, 484–512.

Berger, M.J. and Colella, P., Local adaptive mesh refinement for shock hydrodynamics. *J. Comput. Phys.*, 1989, **82**, 67–84.

Berger, M.J. and Saltzman, J.S., AMR on the CM-2. *Appl. Numer. Math.*, 1994, **14**, 239–253.

Coirier, W.J. and Powell, K.G., An adaptively-refined, Cartesian, cell-based scheme for the Euler and Navier–Stokes equations. *AIAA J.*, 1996, **34**(5), 938–945.

Dally, B.B., Fletcher, D.F. and Masri, A.R., Flow and mixing fields of turbulent bluff-body jets and flames. *Combust. Theory Modelling*, 1998, **2**, 193–219.

De Zeeuw, D. and Powell, K.G., An adaptively refined Cartesian mesh solver for the Euler equations. *J. Comput. Phys.*, 1993, **104**, 56–68.

Dixon-Lewis, G., Computer modeling of combustion reactions in flowing systems with transport. In *Combustion Chemistry*, edited by W.C. Gardiner, pp. 21–126, 1984 (Springer-Verlag: New York).

Douglas, C.C., Ern, A. and Smooke, M.D., Numerical simulation of flames using multigrid methods. In *Iterative Methods in Scientific Computation*, edited by J. Wang, M.B. Allen, B.M. Chen and T. Mathew, **4**, pp. 149–154, 1998 (New Brunswick).

Einfeldt, B., Godunov-type methods for gas dynamics. *SIAM J. Numer. Anal.*, 1988, **25**, 294–318.

Gordon, S. and McBride, B.J., Computer program for calculation of complex chemical equilibrium compositions and applications I. Analysis. Reference Publication 1311, NASA, 1994.

Gropp, W., Lusk, E. and Skjellum, A., *Using MPI*, 1999 (MIT Press: Cambridge, Massachussets).

Groth, C.P.T., De Zeeuw, D.L., Marshall, H.G., Gombosi, T.I., Powell, K.G. and Stout, Q.F., A parallel solution-adaptive scheme for ideal magnetohydrodynamics. *AIAA Pap.*, 1999, 99–3273.

Groth, C.P.T., De Zeeuw, D.L., Gombosi, T.I. and Powell, K.G., Global three-dimensional MHD simulation of a space weather event: CME formation, interplanetary propagation, and interaction with the magnetosphere. *J. Geophys. Res.*, 2000, **105**(A11), 25053–25078.

Laufer, J., The structure of turbulence in fully developed pipe flow, Report 1174, NACA, 1954.

Linde, T., A practical, general-purpose, two-state HLL Riemann solver for hyperbolic conservation laws. *Int. J. Numer. Meth. Fluids*, 2002, **40**, 391–402.

Magnussen, B.F. and Hjertager, B.H., On mathematical modeling of turbulent combustion with special emphasis on soot formation and combustion, 16th Symp. (Int.) on Combustion (1976). Comb. Inst., Pittsburg, Pennsylvania pp. 719–729.

McBride, B.J. and Gordon, S., Computer program for calculation of complex chemical equilibrium compositions and applications II. Users manual and program description, Reference Publication 1311, NASA, 1996.

Northrup, S.A. and Groth, P.T.G., Solution of laminar diffusion flames using a parallel adaptive mesh refinement algorithm. *AIAA Pap.*, 2005, 2005–0547.

Powell, K.G., Roe, P.L. and Quirk, J.J., Adaptive-mesh algorithms for computational fluid dynamics. In *Algorithmic Trends in Computational Fluid Dynmaics*, edited by M.Y. Hussaini, A. Kumar and M.D. Salas, pp. 303–337, 1993 (Springer-Verlag: New York).

Quirk, J.J., An adaptive grid algorithm for computational shock hydrodynamics, Ph.D. thesis, Cranfield Institute of Technology, 1991.

Quirk, J.J. and Hanebutte, U.R., A parallel adaptive mesh refinement algorithm, Report 93–63, ICASE, August 1993.

Roe, P.L., Approximate Riemann solvers, parameter vectors, and difference schemes. *J. Comput. Phys.*, 1981, **43**, 357–372.

Sachdev, J.S., Groth, C.P.T. and Gottlieb, J.J., A parallel solution-adaptive scheme for predicting multi-phase core flows in solid propellant rocket motors. *Int. J. Comput. Fluid Dyn.*, 2005, **19**(2), 157–175.

TNF, http://www.ca.sandia.gov/TNF/.

Turpin, G. and Troyes, J., Validation of a two-equation turbulence model for axisymmetric reacting and non-reacting flows. *AIAA Pap.*, 2000, 2000–3463.

van Leer, B., Tai, C.H. and Powell, K.G., Design of optimally-smoothing multi-stage schemes for the Euler equations. *AIAA Pap.*, 1989, 89-1933-CP.

Westbrook, C.K. and Dryer, F.L., Simplified reaction mechanisms for the oxidation of hydrocarbon fuels in flames. *Combust. Sci. Technol.*, 1981, **27**, 31–43.

Wilcox, D.C., *Turbulence Modeling for CFD*, 2002 (DCW Industries: La Cañada).

Wilke, C.R., A viscosity equation for gas mixtures. *J. Chem. Phys.*, 1950, **18**, 517–519.